Electronic supplementary information (ESI):

Split-anion solvent extraction of light rare earths from concentrated chloride aqueous solutions to nitrate organic ionic liquids

Mercedes Regadío, Tom Vander Hoogerstraete, Dipanjan Banerjee, and Koen Binnemans

Abbreviation list: [A336][NO_3], tricaprylmethylammonium nitrate (Aliquat 336 nitrate form); Cy923, Cyanex 923; [C101][NO_3], trihexyl(tetradecyl)phosphonium nitrate (Cyphos IL 101 nitrate form); D, distribution ratio; E(%), percentage extraction; EG, ethylene glycol; IL, ionic liquid; LO, loaded organic (phase); O/A, volume ratio organic-to-aqueous phases; REE, rare-earth element; RT, room temperature; TBP, tri-n-butyl phosphate; $\boldsymbol{\alpha_B^A}$, separation factor of A from B.

Table of contents

SI 1. Mixtures of TBP and IL-nitrate

When dissolving TBP in the ILs, the extraction efficiencies and distribution ratios of La(III), Ce(III) and Pr(III) did not change significantly with the amount of TBP used (Fig. S1). However, the separation factors slightly decreased with the quantity of TBP, from 1 v% TBP (0.037 mol L^{-1}) (and 1.68 mol L^{-1} [A336][NO_3] or 1.58 mol L^{-1} [C101][NO_3]), to 20 v% TBP (0.73 mol L^{-1}) (and 1.36 mol L^{-1} [A336][NO_3] or 1.28 mol L^{-1} [C101][NO_3]) (Fig. S1). Only two points were obtained in the case of TBP in [C101][NO_3], as explained here below. After measuring different TBP concentrations in [A336][NO_3] (Fig. S1 left) and having observed that the extraction behaviour of [A336][NO_3] is very the similar to the one of [C101][NO_3] (Fig. 1 in the main text), it was decided to measure the two most opposite cases with [C101][NO_3] (Fig. S1, right). As both data points gave similar values between them and between the points of its counterpart TBP in [A336][NO_3], we can expect similar results for intermediate TBP concentration in [C101][NO_3].

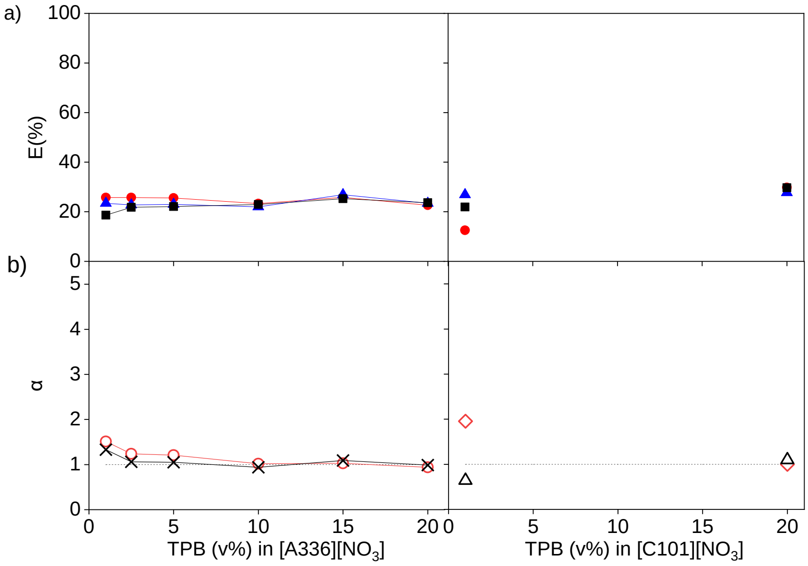

Fig. S1. a)Extraction of La(●), Ce(▲) and Pr(■), and b) separation factors of α^{La}_{Pr} *(O),* α^{Ce}_{Pr} *(X),* α^{Pr}_{La} *(◊) and* α^{Pr}_{Ce} *(Δ), after one contact with different TBP concentrations in [A336][*NO_3*] (left) and [C101][*NO_3*] (right) at 70–80 °C, 3000 rpm, volume O/A 1:1. Chloride feed solution: 2.0, 4.4 and 0.6 g* L^{-1} *of La(III), Ce(III) and Pr(III) (0.05 mol* L^{-1} *total REE), 2 mol* L^{-1} $CaCl_2$*. Distribution ratios: 0.32 ± 0.06 and 0.34 ± 0.11 for [A336][*NO_3*] and [C101][*NO_3*], respectively (average of La(III), Ce(III) and Pr(III)).*

SI 2. Competitive complex formation effect

The effect of the REE concentration in a 2 mol L^{-1} $CaCl_2$ feed solution on the extraction of La(III), Ce(III) and Pr(III) by 20 v% of the extractants in the nitrate ionic liquids was examined. The concentration of REE, of $CaCl_2$ and of Cy923 are the key parameters that determine the loading capacity of the system, on the basis of which the separation could be adjusted. If the concentration of REE increases, to keep the selectivity, the concentration of $CaCl_2$ or of Cy923 should increase (Fig. 2, Fig. 3 and Fig. 4, in the main text). For instance, a 2 mol L^{-1} $CaCl_2$ feed solution with 7 g L^{-1} (0.05 mol L^{-1}) of REE, has relatively high selectivity of Pr from La and of Pr from Ce with 10 v% Cy923 (3.5 and 1.5, Fig. 4). When the feed solution increases its REE content to 40 g L^{-1} (0.29 mol L^{-1}) with the same concentration of $CaCl_2$, the Cy923 in the IL has to go up from 10 to 20 v% to obtained separation factors of Pr from La and of Pr from Ce as high as 4.5 and of 2.5, respectively (Fig. S2). The behaviour in systems with TBP is similar but with lower extraction efficiencies compared to systems with Cy923 in [A336][NO_3] and in [C101][NO_3] (Fig. S2).

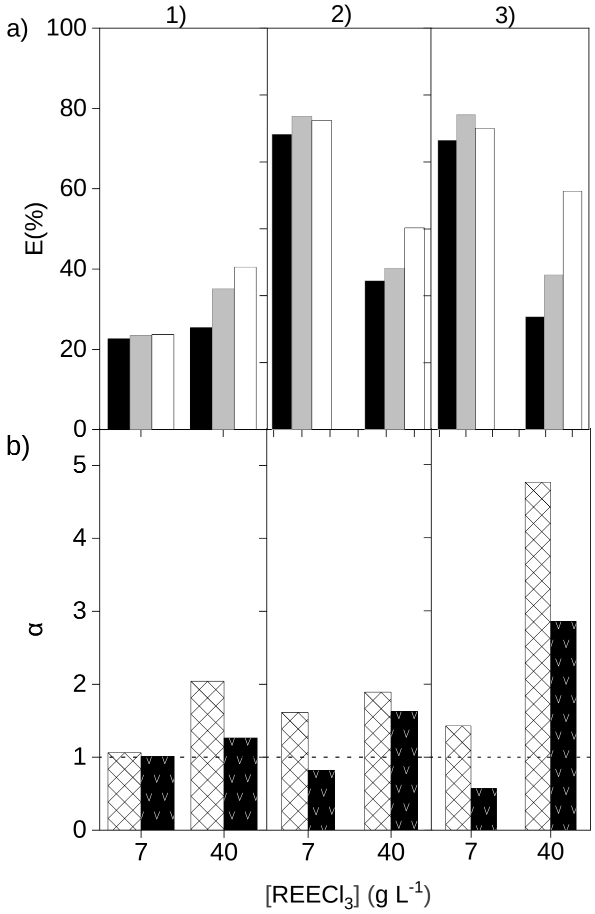

Fig. S2. a) Extraction of La (■), Ce (▒) and Pr (□), and b) separation factors of α_{La}^{Pr} (◊) *and* α_{Ce}^{Pr} (V) *as a function of concentration of REEs in the feed solution, after one contact with three different organic phases: 1) 20 v% TBP in [A336][NO$_3$], 2) 20% Cy923 in [A336][NO$_3$], 3) 20% Cy923 in [C101][NO$_3$]. At 70–80ºC, 3000 rpm, volume O/A 1:1 and 2 mol L^{-1} CaCl$_2$.*

SI 3. Effect of the chloride concentration in a 10 v% ethylene glycol aqueous phase on the extraction of REE

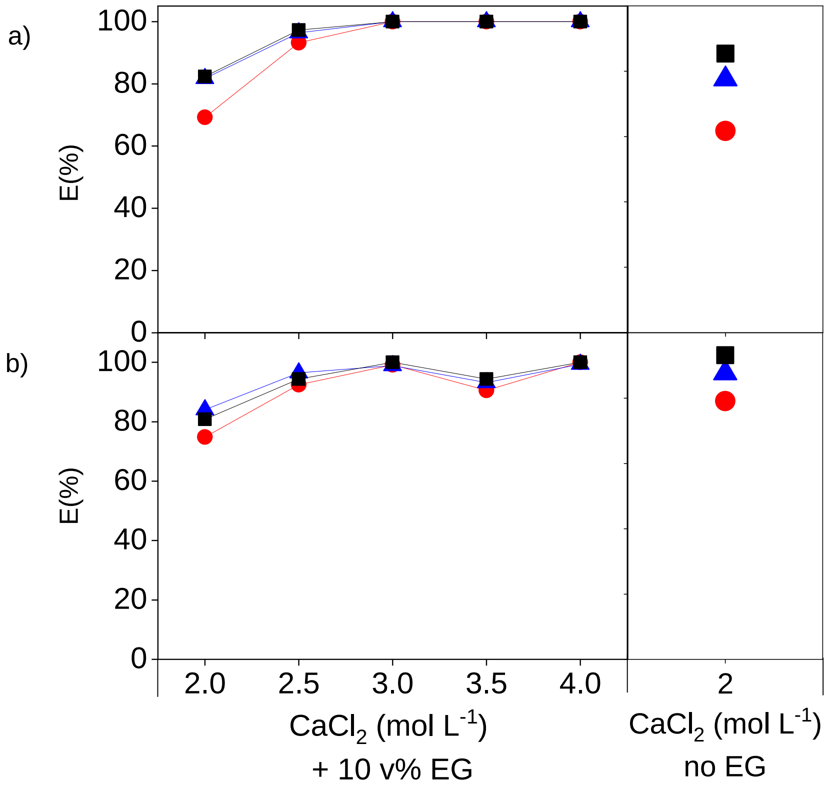

Fig. S3. Extraction of La (●), Ce (▲) and Pr (■), after one contact with 10 w% Cy923 a) in [C101][NO$_3$] and b) in [A336][NO$_3$], as a function of CaCl$_2$ and EG. At 80ºC, 3000 rpm, volume O/A 1:1, chloride feed solution: 1.7, 4.0, 0.6 g L^{-1} of La(III), Ce(III) and Pr(III).

Table S1. Separation factors of Pr(III) from La(III) and from Ce(III) as a function of CaCl$_2$ concentration in a feed solution with 10 v% ethylene glycol.

FEED PHASE (REE + CaCl$_2$ + 10 v% EG)	ORGANIC PHASES			
	10 w% Cy923 in [A336][NO$_3$]		10 w% Cy923 in [C101][NO$_3$]	
CaCl$_2$, mol L^{-1}	α_{La}^{Pr}	α_{Ce}^{Pr}	α_{La}^{Pr}	α_{Ce}^{Pr}
2	1.42	0.80	2.08	1.05
2.5	1.37	0.61	2.59	1.33
3	a	a	c	c
3.5	1.75	1.23	c	c
4	b	a	c	c

[a]100% *E* Pr;[b]100% *E* La, Pr;[c] 100% *E* La, Ce, Pr.

$\alpha_{A,B}$: separation factor of A from B. Calcium chloride feed solution: 1.7, 4.0, 0.6 g L^{-1} of La(III), Ce(III) and Pr(III) and 10 v% ethylene glycol. IL solutions: with 10 w% Cy923 (80ºC, 3000 rpm, volume O/A 1:1).

SI 4. Loading capacity of the organic phases

Reaching the theoretical maximum loading after one contact is difficult. Apart from the volume ratio organic/aqueous phases and the mixing time, the loading of the organic phase depends on the type of REE, its concentration, the number of contacts and the composition of the organic phase. To study this, the loading of the organic phase as a function of the number of contacts, the element extracted and Cy923/[C101][NO_3] composition was studied. The tests were carried out with four contacts, the REEs La(III), Ce(III) and Pr(III) in 3.26 mol L^{-1} $CaCl_2$ (solution B, C and D) and five different proportions of Cy923 and [C101][NO_3] (Section 2.2). The loading yield ($\%LY$) was used to express the efficiency of the uptake of an element by the organic phase after solvent extraction (eqn S1).

$$\%LY_A = \frac{[A]_{eq,\mathrm{org}}}{[A]_{LC}} \times 100 \qquad \text{(S1)}$$

where $[A]_{eq,org}$ represents the concentration of an element A in the organic phase at equilibrium and $[A]_{LC}$ the loading capacity or maximum amount of element A that the organic phase can accommodate under the tested conditions.

In the case of the dependence on the type of REE, the lowest loadings were for La(III) compared to Ce(III) and Pr(III), for all the organic phases and contacts (Fig. S4a–c and Fig. S5). The more Cy923, the higher preference for the loading with Ce(III) and Pr(III), compared to La(III). At a volume phase ratio of 1:1 O/A, generally between 50–80% loading yield (LY) was achieved after the 1st contact, and between 80−100% after the 2nd contact, depending on the REE and the organic phase composition (Table S2). From the 2nd to the 3th contact the increase in the loading was much less important (Fig. S5). This was especially the case for the REE with higher affinities for organic phases that contain Cy923 (like Ce or Pr), meanwhile REE with lower affinities, thus, lower extraction and loadings (i.e., the lightest one, La) needed more contacts to reach the maximum loading capacity (Fig. S4 and Fig. S5). In the case of the dependence on the composition of the organic phase, the higher the content of Cy923 is, the higher the overall loading capacities are (Fig. S5) and the lower the loadings of La(III) are (Fig. S4a–c). The fact that [C101][NO_3] on its own (0/100) reached the maximum loading before any of the Cy923 combinations, is related to the lower loading capacity of [C101][NO_3], which allows reaching the equilibrium faster (Fig. S4d–f and Fig. S5a). No differences were found between the organic phases composed of 75/25 and 100/0 Cy923/[C101][NO_3] (Fig. S4).

Table S2. Loading yields (LY, %) and loading capacities (LC, g L^{-1}) of five organic phases from three individual REE feed solutions (3.26 mol L^{-1} $CaCl_2$).

Volume ratio:	LY, % (1st contact)			LY, % (2nd contact)			[a] LC, g L^{-1}		
Cy923/[C101][NO_3]	La	Ce	Pr	La	Ce	Pr	La	Ce	Pr
0/100	80	76	62	100	100	100	8	9	9
25/75	60	59	59	90	101	89	30	32	34
50/50	60	60	58	86	97	83	40	44	44
75/25	49	58	53	79	95	88	49	51	51
100/0	50	56	51	80	96	91	47	53	51

[a] LC: after contacting the organic phase four times with new/fresh feed of concentrated chloride aqueous solutions, at RT, 300 rpm, 8h (1st, 2nd and 3th contacts: volume phase 1:1 O/A, 4th contact 1:2.85 O/A).

Polynomial fitting in the percentage volume of Cy923 and the loading capacity

The loading capacity (LC) of the organic phase from a 3.26 mol L^{-1} $CaCl_2$ feed solution, can be estimated as a function of the percentage volume of Cy923 in [C101][NO_3], with the eqn S2, and Table S3.

$$LC_{\mathrm{RE}} = a_0 + a_1 x + a_2 x^2 \qquad \text{(S2)}$$

where LC_{RE} is the loading capacity with a RE in the organic phase (g L^{-1} or mol L^{-1}) and x is the percentage volume of Cy923 in [C101][NO_3].

Table S3. Polynomial fitting in the percentage volume of Cy923 and the loading capacity

RE (Adj. R^2)	LC, $g\ L^{-1}$			LC, $mol\ L^{-1}$		
	Constants	Value	Standard error	Constants	Value	Standard error
La(III) (0.9914)	Intercept,a_0	8.327	± 1.464	Intercept,a_0	0.05994	± 0.01052
	a_1	0.933	± 0.069	a_1	0.00672	± 0.00050
	a_2	-0.005	± 0.001	a_2	-0.00004	± 0.00000
Ce(III) (0.9937)	Intercept,a_0	9.471	± 1.352	Intercept,a_0	0.06777	± 0.00965
	a_1	0.989	± 0.064	a_1	0.00708	± 0.00046
	a_2	-0.006	± 0.001	a_2	-0.00004	± 0.00000
Pr(III) (0.9837)	Intercept,a_0	9.760	± 2.125	Intercept,a_0	0.06951	± 0.01506
	a_1	1.023	± 0.101	a_1	0.00723	± 0.00071
	a_2	-0.006	± 0.001	a_2	-0.00004	± 0.00001

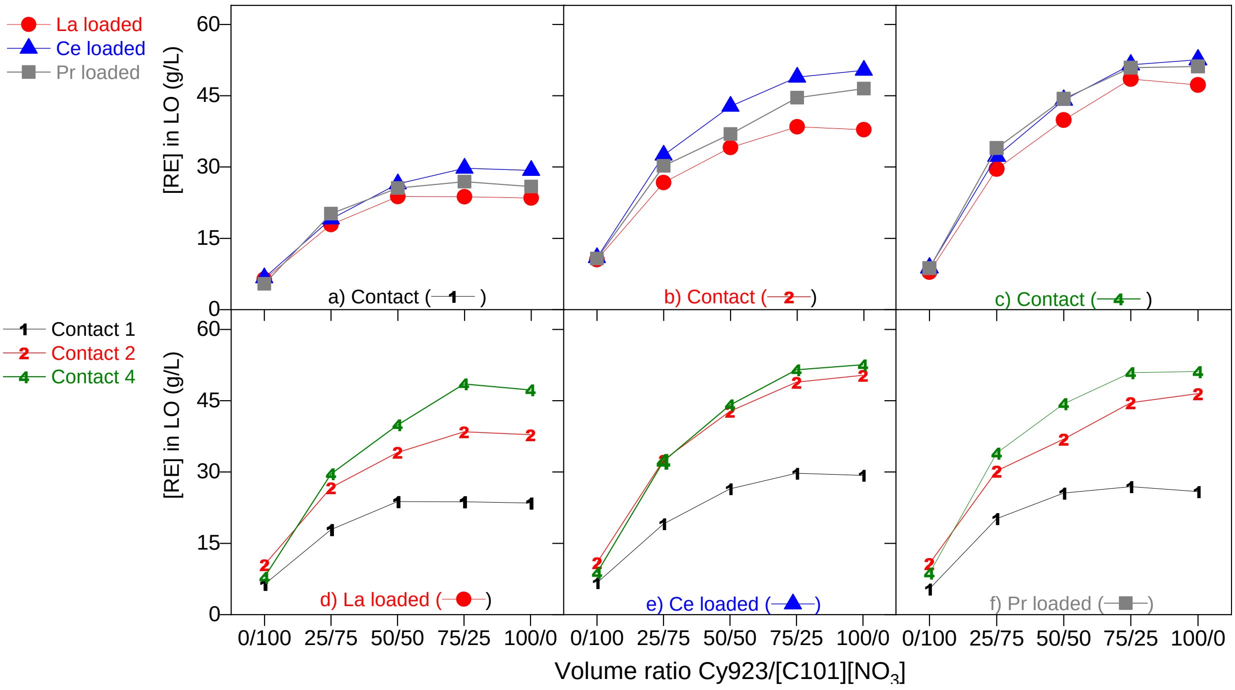

Fig. S4. Concentration of La, Ce and Pr in LO as a function of the volume ratio Cy923/[C101][NO$_3$], after the 1st, the 2nd and the 4th contacts with new fresh feed solutions. Four consecutive contacts with fresh solutions B, C and D at O/A 1:1, 1:1 , 1:1 and 1:2.85, 8 h, RT, 300 rpm.

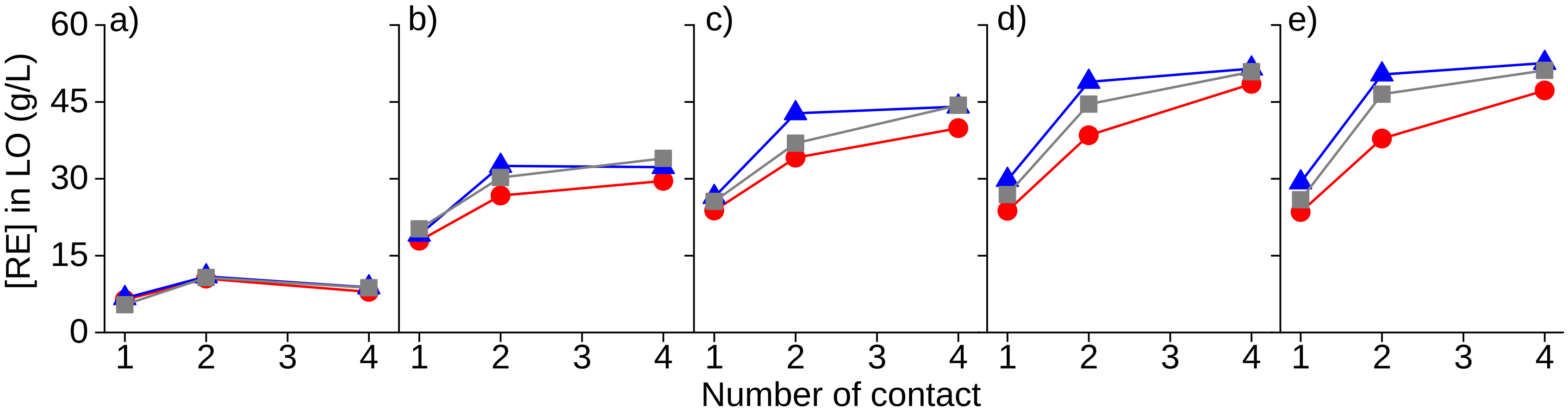

Fig. S5. Concentration of La (●), Ce (▲) and Pr (■) in LO as a function of the number of contacts and the volume ratio Cy923/[C101][NO$_3$]: a) 0/100, b) 25/75, c) 50/50, d) 75/25, e) 100/0. Four consecutive contacts with fresh solutions B, C and D at O/A 1:1, 1:1 , 1:1 and 1:2.85, 8 h, RT, 300 rpm.

SI 5. Methodology of Extended X-ray Absorption Fine Structure (EXAFS) and X-ray Absorption Near Edge Structure (XANES)

X-ray Absorption Near Edge Structure (XANES) is related to the interaction with the first neighbours of the absorbing element, while Extended X-ray Absorption Fine Structure (EXAFS) allows the determination of distances, coordination numbers and degree of thermal and/or structural disorder of the local structure (first few atomic coordination shells) surrounding the absorbing atom. Both spectroscopic techniques offer information on the local atomic coordination to distances of 0.5 nm and sometimes until of 0.8 nm. The energy of the X-ray beam was tuned by a double-crystal monochromator operating in fixed-exit mode using a Si(311) crystal pair. The measurements were done in transmission mode using Ar/He gas filled ionisation chambers. The organic samples (Table S4) were hold in plastic cuvettes of 1 cm wide and X-rays travel distances of 3, 6 or 10 mm path lengths.

Table S4. Composition of the organic samples measured by X-ray absorption spectroscopy

Name in the graphs	Volume ratio Cy923/C101 (organic phase)	Molar ratio Cy923/C101 (organic phase)	REE	Concentration of REE in LO		EXAFS could be solved[a]
				g L^{-1}	mol L^{-1}	
Nitrate organic samples after metal-loaded from concentrated **chloride** aqueous solutions						
La1	0/100	0/1.6	La	7.9	0.06	✓
Ce2	0/100	0/1.6	Ce	8.8	0.06	✓
La4	25/75	1/1.85	La	29.6	0.21	
La7	50/50	1.61/1	La	39.9	0.29	✓
Ce8	50/50	1.61/1	Ce	44.1	0.31	✓
La10	75/25	4.76/1	La	48.5	0.35	
Anion-free and phosphonium-free organic samples after metal-loaded from concentrated chloride aqueous solutions						
La13	100/0	2.6/0	La	47.2	0.34	✓
Ce14	100/0	2.6/0	Ce	52.6	0.38	✓
Pr15	100/0	2.6/0	Pr	51.1	0.36	✓
Nitrate organic samples after metal-loaded from concentrated-**nitrate** aqueous solutions						
$[La(NO_3)_5]^{2-}$	0/100	0/1.6	La	70	0.50	✓
$[Ce(NO_3)_5]^{2-}$	0/100	0/1.6	Ce	70	0.51	✓

Cy923 = Cyanex 923, C101 = $[C101][NO_3]$, LO = loaded organic phase

[a] Sufficient data quality of the spectrum in the EXAFS region.

Standard procedures were used for pre-edge subtraction and data normalisation in order to isolate the EXAFS function (χ). The isolated EXAFS oscillations, accomplished by a smoothing spline or by a through the knots function realised by the program Viper [1], were k^4 – weighted and Fourier transformed over the k-range using a Kaiser – Bessel window function. The data were fitted using the *ab initio* code FEFF 7.0, which was used to calculate the theoretical phase and amplitude functions that subsequently were used in the non-linear least-squares refinement of the experimental data.[2] Fitting of the data with the model was performed in R-space. Estimated errors are shown between parentheses for the last significant digit and calculated by VIPER. The amplitude reduction factor (S_0), to correct all effects that reduce the amplitude of the signal, was fixed for all fits at 0.9.

SI 6. Interpretation of EXAFS and XANES spectra

EXAFS and XANES were used to determine the structures and differences of REE complexes in the loaded organic phases shown in Table S4. The K-edge of lanthanum, cerium and praseodymium were measured. Unfortunately, the two platinum-coated mirrors, before and after the monochromator, significantly absorbed the X-ray radiation at these energies (> 30 keV), for an acceptance angle of about 2 mrad. Thus, the X-ray beam intensity dropped sharply, what resulted in noisy EXAFS spectra, especially for the samples with low concentrations of REE. Following are the data that could be successfully solved for the determination of the REE speciation: (1) lanthanum and cerium extracted by [C101][NO_3] from concentrated chloride aqueous solutions, (2) lanthanum and praseodymium extracted by Cy923 from concentrated chloride aqueous solutions and (3) cerium extracted by a 50/50 v/v mixture of Cy923/[C101][NO_3] from concentrated chloride aqueous solutions. In addition, lanthanum and cerium extracted by [C101][NO_3] from concentrated-nitrate aqueous media, were also measured for comparison to the chloride aqueous media (i.e., split-anion extraction). All EXAFS data could be fitted with single-scattering, neglecting the scattering pathways from three or more atoms and any angular information. All EXAFS data could be fitted with single-scattering, neglecting the scattering pathways from three or more atoms and any angular information.

SI 6.1 REE extracted by [C101][NO_3] from concentrated chloride or nitrate aqueous solutions

The Fourier transform (FT) of lanthanum extracted from chloride media to [C101][NO_3] could be fitted by incorporating only a La–O single scattering path resulting in a bond length of 2.633(1) Å and a coordination number of 6.9(1) (Fig. S6.a, Fig. S7.a, Table S5). As noted in the main text, the error on the coordination number can be quite large in EXAFS analysis, and a coordination number of 6.9 might not be the correct value. The average bond length La–O found here was significantly longer than the bond length for hydrated $[La(H_2O)_9]^{3+}$ (± 2.56 Å) obtained by Persson et al.[3] One explanation might be the existence of an outer sphere complex of La with either NO_3^- or Cl^- ions because this would result in a partial negative charge on the H_2O molecules. In such a case, the OH bond distance would become longer because of coordination (H bonding) with the NO_3^- molecule and thus the bond distance between the La–O ions would increase. This could be the case in the second coordination sphere, but the hypothesis was discarded for the first coordination. After incorporating a second sphere of nitrogen atoms for fitting the peak and constraining the degeneracy to the number of oxygen atoms (number of oxygen atoms = 2× number of nitrogen atoms), the results for the first coordination sphere gave unrealistic long or short La–N bond lengths. It was also not possible to fit an outer coordination sphere of Cl^-. Thus, no nitrate or chloride ions, but only water molecules were found in the first coordination sphere of lanthanum.

This was not the case when lanthanum was extracted from nitrate instead of chloride aqueous medium to the nitrate organic medium. The FT of lanthanum extracted from nitrate feed solutions to [C101][NO_3] (Fig. S8) showed an intense, very specific second peak which was due to the single and multiple scattering paths involving the nitrogen and oxygen atoms not coordinating to the lanthanide ion. This second peak due to N–O in the species $[La(NO_3)_5]^{2-}$, was not present in the FT from chloride feed solutions (Fig. S7), what laid in the fact that $[La(H_2O)_7]^{3+}$ instead of $[La(NO_3)_5]^{2-}$was the extractable complex in the first case (split-anion extraction).

The same analysis done for lanthanum was done on the cerium loaded organic phase. The FT of cerium extracted from chloride media to $[C101][NO_3]$ could be fitted by including a Ce–O path with a bond length of 2.595(2) Å and a coordination number of 9.4(2) (Fig. S6.b, Fig. S7.b, Table S5). The Ce–O bond found was also longer than the average bond lengths for cerium dissolved in water (± 2.526).[3] Again, fitting the peak after incorporating a second sphere of nitrogen or chloride atoms that would coordinate to cerium resulted in unreasonable results. As was the case with lanthanum, when cerium was extracted from nitrate instead of chloride aqueous medium, an intense, very particular second peak due to N–O, indicated the species $[Ce(NO_3)_5]^{2-}$

In conclusion, the extraction of La(III) and Ce(III) by $[C101][NO_3]$ from concentrated chloride aqueous media occurred via hydrated lanthanide species, cations which might be stabilized in neutral or anion complexes, by nitrate anions no closer than in the second coordination sphere, as follows: $[(Ln(H_2O)_x)(NO_3)_y]^{3-y}$

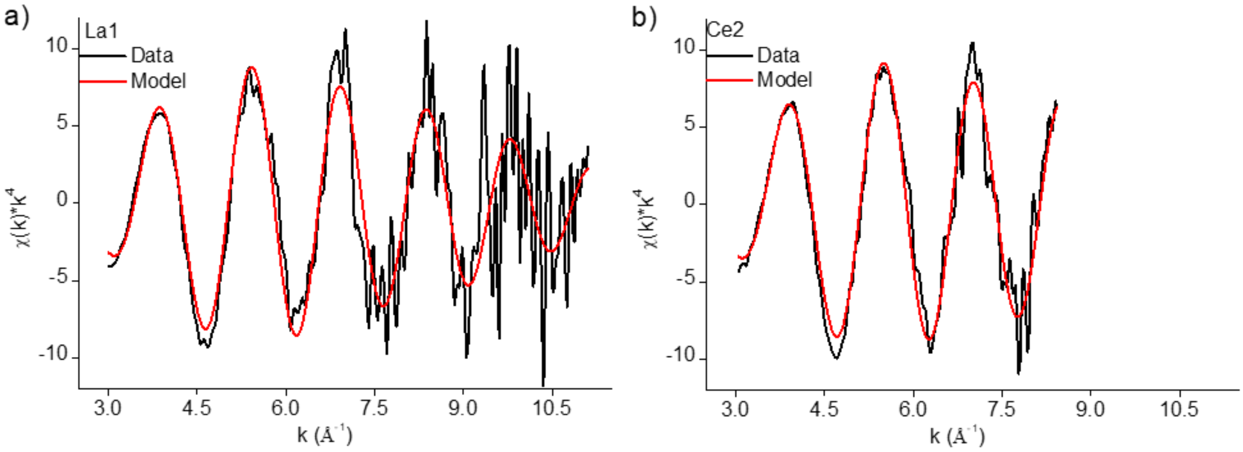

Fig. S6. EXAFS function χ(k)k^4 and model of the hydrated (1st coordination) complexes a) $[La(H_2O)_7]^{3+}$ and b) $[Ce(H_2O)_9]^{3+}$, extracted by $[C101][NO_3]$ from chloride aqueous solutions.*

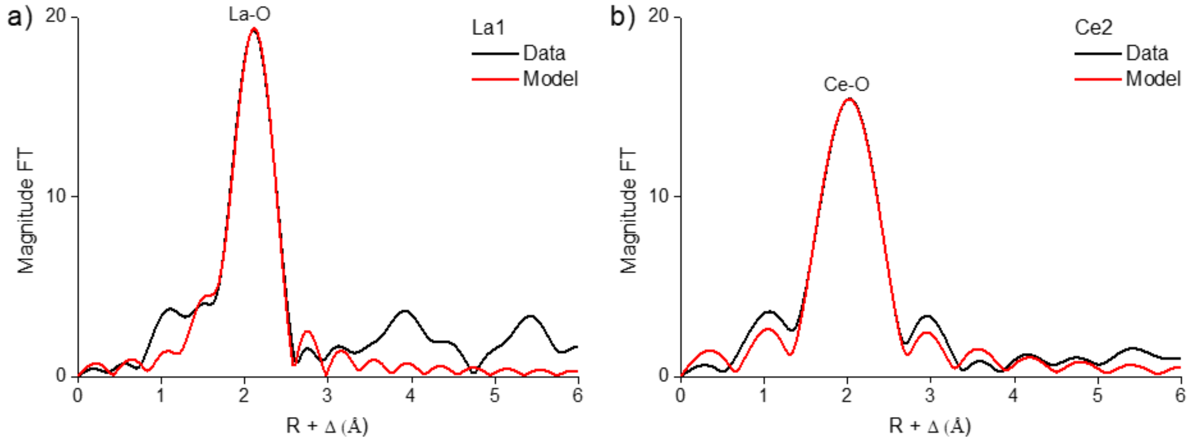

*Fig. S7. Conversion of EXAFS function*k^4 to R-space. FT data and model of the hydrated (1st coordination) complexes a) $[La(H_2O)_7]^{3+}$ and b) $[Ce(H_2O)_9]^{3+}$, extracted by [C101][NO$_3$] from chloride aqueous solutions.*

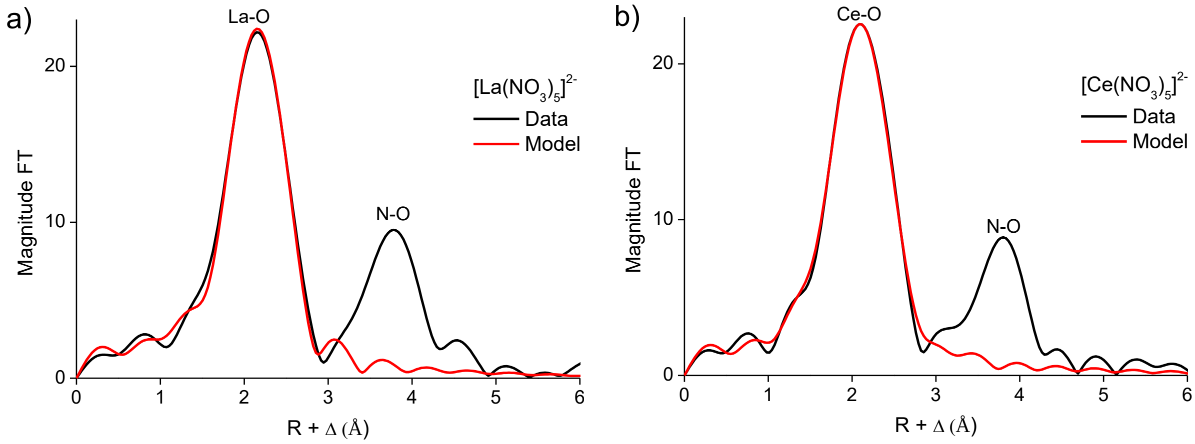

*Fig. S8. Conversion of EXAFS function*k^4 to R-space. FT data and model of the complex a) $[La(NO_3)_5]^{2-}$and b)$[Ce(NO_3)_5]^{2-}$extracted by [C101][NO$_3$] from **nitrate** aqueous solutions.*

Table S5. Fitting results of the FT data (derived from the EXAFS function) of the lanthanum and cerium complexes extracted by [C101][NO$_3$] from concentrated chloride aqueous solutions.

		Data in this work			Persson et al. (2008)[a]		R difference
	Path	N	R (Å)	σ^2 (Å^2)	N	R (Å)	R_{here} - $R_{Persson}$
La	La–O	6.9(1)	2.633(1)	0.012(2)	9	±2.560	0.073
Ce	Ce–O	9.4(2)	2.595(2)	0.011(4)	9	± 2.526	0.069

(La–Cl, La–N, La–P and Ce–Cl, Ce–N, Ce–P not found)

---

[a] Data of La and Ce dissolved in water, $La(H_2O)_9$, $Ce(H_2O)_9$[3].

N: degeneracy of a scattering path, R: half path length (for a single scattering path, the bond length between the absorber and backscatterer atoms), σ^2: Debye-Waller factor (mean-square disorder in R).

SI 6.2 REE extracted by Cy923 from concentrated chloride aqueous solutions

The EXAFS and FT spectrum of lanthanum extracted from chloride media towards Cy923 showed two intense peaks (Fig. S9.a and Fig. S10.a). The first peak could be fitted by 3.4(1) oxygen and 3 chlorine atoms, linked to lanthanum (Table S6). The coordination number of lanthanum was constrained to three chlorine atoms, as three Cl^- have to be co-extracted to the organic phase in order to obtain charge neutrality and there were no other anion solvating molecules present. The second peak could be fitted by a single scattering path La–P resulting in a degeneracy of 2.7 (Table S6). The slightly misfit in the second peak of the FT (Fig. S10.a) might be due to the data quality and the other contributions in this region such as the slightly longer three-leg and four-leg scattering paths involving the almost linear Ln–O=P bonds. The bond lengths and coordination numbers of La–O, La–Cl and La–P (Table S6) were in good agreement with the crystal structure of tris(4-(diphenylphosphoryl)morpholine)-trichloro–lanthanum(III) monohydrate.[4] Therefore, the lanthanum complex formed in the organic phase composed entirely of Cy923, was $LaCl_3 \cdot 3Cy923$. At lower *k*-ranges, the fit was rather poor because of the significant multielectron excitation at 39032 eV in the case of lanthanum which made post-edge background subtraction (μ_0) more difficult (Fig. S11).

When the praseodymium extracted from chloride media towards Cy923 was measured, the same complex (with praseodymium as central metal atom) than in the previous case of lanthanum was determined (Fig. S9.b, Fig. S10.b). The number of oxygen atoms coordinating to praseodymium was found to be 2.7 at a distance of 2.298 Å and the number of chlorine atoms was constrained to be 3 at 2.633 Å (Table S6). These distances were about 0.05 and 0.09 Å smaller than those found in the crystal structure of trichloro-tris(hexamethylphosphoramide)–praseodymium(III) [5]. The degeneracy of the Pr–P scattering path was found to be too high (five instead of three), because of the data quality and other contributions in this region such as the slightly longer three- and four-leg scattering paths involving the almost linear Pr–O=P bonds and the smaller *k*-range used for deriving the FT in comparison to the analysis on lanthanum.

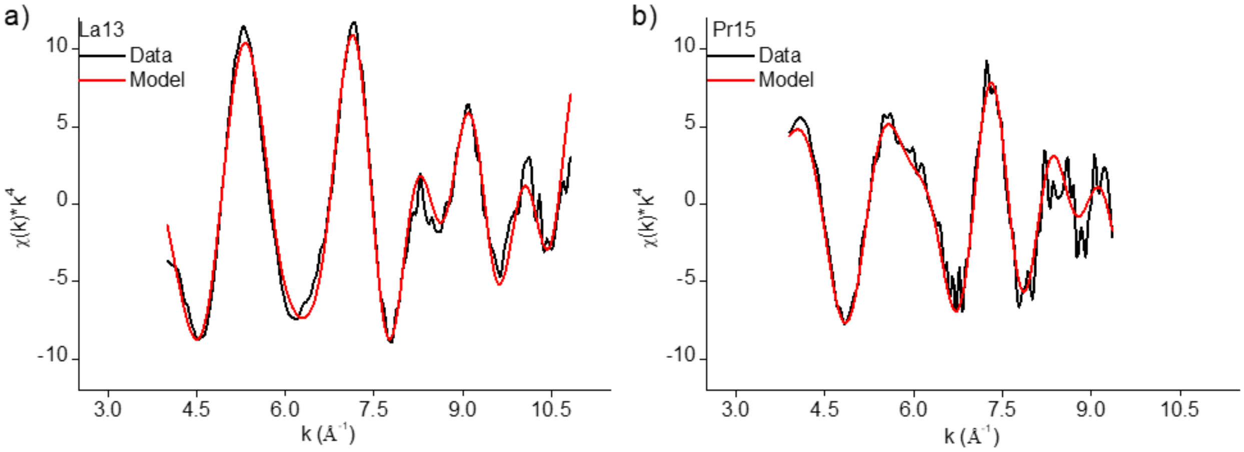

Fig. S9. EXAFS function χ(k)k^4 and model of the complexes a) $LaCl_3$·3Cy923 and b) $PrCl_3$·3Cy923, extracted by Cy923 from chloride aqueous solutions.*

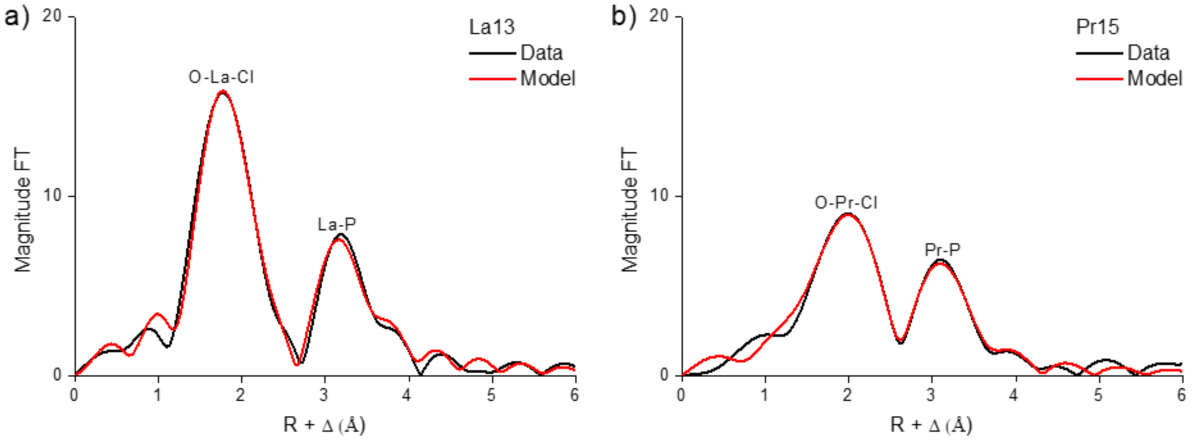

Fig. S10. Conversion of EXAFS functionk^4 to R-space. FT data and model of the complexes a) $LaCl_3$·3Cy923 and b) $PrCl_3$·3Cy923, extracted by Cy923 from chloride aqueous solutions.*

Table S6. Fitting results of the FT data (derived from the EXAFS function) of the lanthanum and praseodymium complexes extracted by Cy923 from concentrated chloride aqueous solutions.

		Data in this work			Gholivand and Mahzouni(2012)[a] Radonovich and Glick (1973)[b]		R difference
	Path	N	R (Å)	σ^2 (Å^2)	N	R (Å)	$R_{here} - R_{Gholivand}$
La	La–O	3.4(1)	2.402(3)	0.005(1)	3	2.399[a]	0.003
	La–Cl	3*	2.708(3)	0.009(1)	3	2.764[a]	-0.056
	La–P	2.7(3)	3.896(4)	0.004(1)	3	3.829[a]	0.067
Pr	Pr–O	2.7(1)	2.298(3)	0.011(1)	3	2.354[b]	-0.056
	Pr–Cl	3*	2.633(2)	0.010(1)	3	2.721[b]	-0.088
	Pr–P	5.0(3)[c]	3.889(3)	0.009(1)	3	3.806[b]	0.083
	(La–N and Pr–N not found)						

---

[a] Crystal structure of tris(4-(diphenylphosphoryl)morpholine)-trichloro–lanthanum(III) [4]

[b] Crystalstructure of trichloro-tris(hexamethylphosphoramide)–praseodymium(III) [5]

[c] Large error due to the three- and four-leg scattering paths Pr–O=P bonds and the smaller *k*-range.

*constrained. N: degeneracy of a scattering path, R: half path length (for a single scattering path, the bond length between the absorber and backscatterer atoms), σ^2: Debye-Waller factor (mean-square disorder in R).

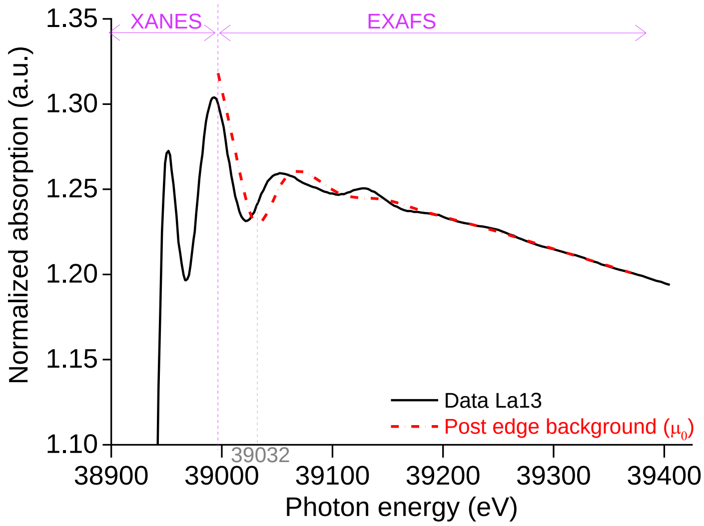

Fig. S11. Post edge background function (μ_0) used on the data of lanthanides extracted by Cy923 from chloride aqueous solutions. Demarcation of XANES and EXAFS regions on the bottom of the figure.

SI 6.3 REE extracted by 50/50 Cy923/[C101][NO$_3$] from concentrated chloride aqueous solutions

Only one good EXAFS spectrum in an organic phase containing 50 v% of Cy923 and 50 v% of [C101][NO$_3$], after extraction from concentrated chloride media, could be measured: the one that corresponds to cerium (Fig. S12.a). The FT showed three peaks of ligands coordinating to the cerium center (Fig. S12.b). The first peak could be fitted by nine oxygen atoms at an average Ce–O bond distance of 2.388(2) Å (Table S7). This distance was very short in comparison to the average Ce–O distance found in the crystal structure of tris(nitrato)-tris(triethylphosphine oxide)–cerium(III).[6] The following peak could be fitted by a second sphere of nitrogen atoms constrained to three nitrate ligands coordinated to cerium. The half path length Ce–N found (2.964(2) Å) was also shorter than the one in the just above-cited crystal structure (Table S7). This FT peak of the nitrogen atoms could not be fitted by chlorine atoms, as Ce–Cl bonds are found at shorter distances (2.6 Å). This combination of oxygen and nitrogen atoms coordinating to cerium were too close to see two completely separated peaks in Fig. S12.b. The high Debye-Waller factors of both first and second spheres (σ^2= 0.020 and 0.022 Å^2) were due to the difference in distance between the oxygen atoms of nitrate (from [C101][NO$_3$]) and those of phosphorus (from Cy923). Finally, a third sphere containing 1.5(1) phosphorus atoms was found at a distance of 3.874(4) Å from cerium (Table S7). Although this bond distance Ce–P was in agreement with the crystal structure of tris(nitrato)-tris(triethylphosphine oxide)–cerium(III),[6] the effective Ce–P distance might be shorter and consequently, the calculated Ce–P degeneracy might differ from the real value. This is because two other paths contributing to this last peak were not fitted, and as these were longer than the Ce–P paths, the resulting Ce–P distance was longer than it should be, to compensate the missing paths. These paths were the three- and four-leg scattering paths to the non-coordinating nitrogen and oxygen atoms of nitrate and the three- and four-leg scattering paths of the phosphorus and oxygen atoms of Cy923.

Overall, it can be concluded that the main cerium complex at 50/50 Cy923/[C101][NO_3] was $Ce(NO_3)_3\cdot 3Cy923$ but there are probably minor amounts of other species, like $[Ce(H_2O)_9]^{3+}$ and CeCl3·3Cy923, which were found in pure [C101][NO_3] and pure Cy923, respectively (Sections S6.1 and S6.2).

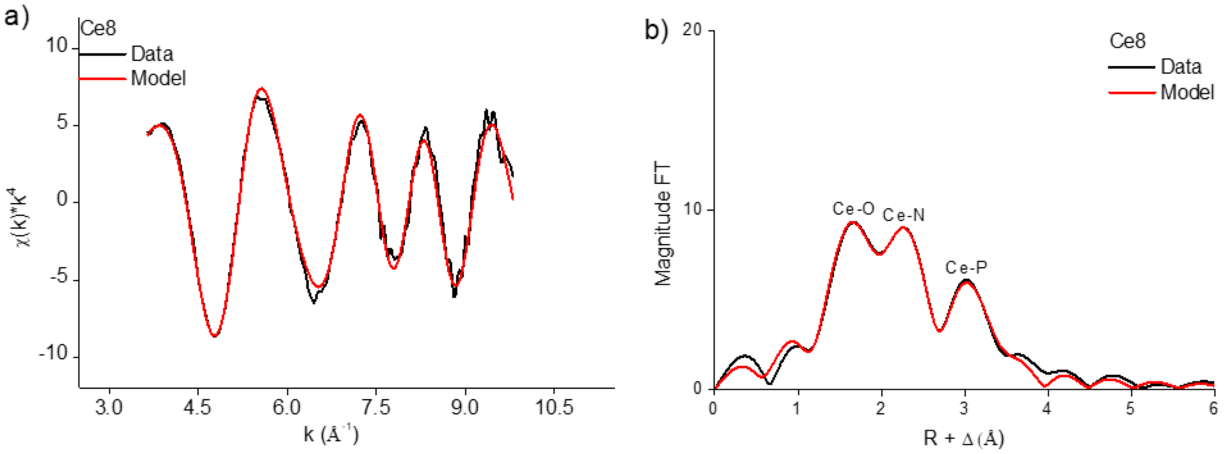

Fig. S12. a) EXAFS function $\chi(k)*k^4$ and model and b) Conversion to R-space into FT data and model, of the complex $Ce(NO_3)_3\cdot 3Cy923$ extracted by a 50/50 mixture of Cy923/[C101][NO_3] from chloride aqueous solutions.

Table S7. Fitting results of the FT data (derived from the EXAFS function) of the Ce complexes extracted by 50/50 volume Cy923/[C101][NO_3] from concentrated chloride aqueous solutions.

	Data in this work			Bowden et al. (2012)[a]		R difference
Path	N	R (Å)	σ^2 ($Å^2$)	N	R (Å)	R_{here} - R_{Bowden}
Ce–O	9.0(5)	2.388(2)	0.020(1)	8-10	2.591(5)-2.582(5)	-0.20
Ce–N	3*	2.964(2)	0.022(2)	3.06	3.06	-0.10
Ce–P	1.5(1)[b]	3.874(4)[b]	0.007(1)			
(Ce–Cl not found)						

---

[a] Crystal structure of tris(nitrato)-tris(triethylphosphine oxide)–cerium(III).[6]

[b] Large error due to two non-fitted scattering paths: Ce–N–O and Ce–O=P bonds(three- and four-leg).

*constrained. N: degeneracy of a scattering path, R: half path length (for a single scattering path, the bond length between the absorber and back-scatterer atoms), σ^2: Debye-Waller factor (mean-square disorder in R).

REFERENCES

1. K. V. Klementev, *Nucl. Instrum. Methods Phys Res A*, 2000, **448**, 299-301.
2. M. Newville, *J. Synchrotron Radiat.*, 2001, **8**, 96-100.
3. I. Persson, P. D'Angelo, S. De Panfilis, M. Sandstrom and L. Eriksson, *Chem. Eur. J.*, 2008, **14**, 3056-3066.
4. K. Gholivand and H. R. Mahzouni, *Inorg. Chim. Acta*, 2012, **386**, 8-12.
5. L. J. Radonovich and M. D. Glick, *J. Inorg. Nucl. Chem.*, 1973, **35**, 2745-2752.
6. A. Bowden, K. Singh and A. W. G. Platt, *Polyhedron*, 2012, **42**, 30-35.